Organic Electronics 13 (2012) 1409–1419

Contents lists available at SciVerse ScienceDirect

Organic Electronics

journal homepage: www.elsevier.com/locate/orgel

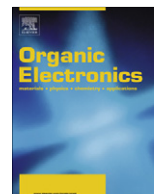

Defect profiling in organic semiconductor multilayers

Priya Maheshwari [a], P.K. Pujari [a,*], S.K. Sharma [a], K. Sudarshan [a], D. Dutta [a], S. Samanta [b], A. Singh [b], D.K. Aswal [b], R. Ajay Kumar [c], I. Samajdar [c]

[a] Radiochemistry Division, Bhabha Atomic Research Centre, Mumbai 400085, India
[b] Technical Physics Division, Bhabha Atomic Research Centre, Mumbai 400085, India
[c] Department of Metalurgical Engineering and Material Science, Indian Institute of Technology Bombay, Mumbai 400076, India

ARTICLE INFO

Article history:
Received 2 January 2012
Received in revised form 21 March 2012
Accepted 27 March 2012
Available online 20 April 2012

Keywords:
Positron annihilation spectroscopy
Organic semiconductors heterostructures
Interfaces
Defects

ABSTRACT

Defect depth profile study has been carried out in organic semiconductor (OSC) multilayers to characterize the buried interfaces and layers using beam based positron annihilation spectroscopy. The bilayer and trilayer heterostructures (*p*–*n*, *p*–*p* and *n*–*p*–*n*) comprise of organic–organic and organic–inorganic (substrate) interfaces. Our study reveals the presence of defects at the interfaces whose concentration is seen to vary with the layer thickness. The *S*–*W* correlation has been used to examine the effect of organic materials as well as thickness of the layers on the defect microstructure in multilayers. The nature and type of defects in *p*–*p* bilayer are seen to be different as compared to *p*–*n* and *n*–*p*–*n* multilayers. Positron mobility in OSC layers has been calculated from the fitted diffusion length which is seen to be of the same order as the effective mobility of charge carrier obtained from the measured current density–voltage (*J*–*V*) characteristics. The role of structural defects and the intrinsic electric field at the interfaces on positron systematics is also examined. Positron diffusion modeling together with experimental data suggests that the defect at the interfaces has a stronger influence on the positron systematics than the intrinsic electric field across organic–organic interfaces.

© 2012 Elsevier B.V. All rights reserved.

1. Introduction

Molecular electronics has attracted worldwide attention due to the advantages over silicon technology in terms of low-cost, ease of processing, compatibility with wide range of substrates, large area and ease of tailoring the material characteristics. The fundamental properties and applications of organic molecules in electronic and opto-electronic devices have been an issue of intensive research since many years. Variety of organic molecules are being used as active material in devices such as organic transistors [1], organic photovoltaic cells (PVs) [2,3], organic light emitting diodes (LEDs) [4] and organic memory devices [5]. These devices are essentially multilayered structures consisting of heterojunctions of organic–organic, metal–organic as well as organic–inorganic materials. The understanding of interface properties holds the key to ascertain working mechanism as well as performance of the devices. The growth and crystalline order of interfacial semiconducting layers are believed to dictate device performance. For example, nature of interface determines the fate of excitons to be either stabilized (for efficient LEDs) or destabilized (for efficient PVs) at the interface. In organic spintronics, interface between a ferromagnetic metal contact and an organic semiconductor (OSC) is important for the spin transfer from one material to another [6,7]. The charge transport across the interface between various organic and inorganic components and light absorption/emission characteristics of the device are believed to be influenced by structural and electronic properties of the interface. A lot of work focusing on the engineering of interfacial properties has been carried out to achieve the best possible performance of organic devices [8,9]. While most of these

* Corresponding author. Tel.: +91 22 25594575; fax: +91 22 25505151.
E-mail address: pujari@barc.gov.in (P.K. Pujari).

1566-1199/$ - see front matter © 2012 Elsevier B.V. All rights reserved.
http://dx.doi.org/10.1016/j.orgel.2012.03.032

studies deal with electronic band alignment at organic–organic interfaces [10–12], there are reports on the structural and morphological aspects of film growth and interfacial characteristics using scanning probe microscopies, X-ray absorption and diffraction techniques. However, there is no systematic study on the open volume defects, especially at the interfaces which are believed to influence the charge transport properties. In the present work we have carried out a systematic depth profiling of defects in different OSC multilayers comprising of organic–organic and organic–inorganic interfaces using a slow positron accelerator. The objective has been two fold; one, to explore and understand the positron systematics, two, extract useful information on the microstructure across buried interfaces.

Positron annihilation spectroscopy (PAS) is a sensitive technique to probe atomic order defects/open volumes as compared to conventional defect characterization techniques. This is due to the unique repulsive force between the positrons and ion cores that facilitates localization of positrons in the open volume defects such as vacancies or voids in metals or semiconductors with sensitivity in the range of a few ppm to size as small as a monovacancy. The underlying manifestation that is indexed in positron defect spectroscopy is the increase in the life-time of positron/Ps upon localization in defects because of the lowering of electron density as compared to bulk. The momentum distribution of electrons in defects differs from the bulk i.e. the measured momentum distribution is considerably narrowed down when a positron is trapped in a defect. This is reflected in the Doppler broadening of annihilation gamma-rays. Conventional positron spectroscopies use ^{22}Na source which is sandwiched between the samples under study. However, due to large spread in positron energy, it cannot be used for depth profiling studies as well as the study of ultrathin films. The slow positron accelerator, on the other hand, provides monoenergetic beam of positrons that can be used to carry out depth profiling studies even in ultrathin films. Also, it enables probe of defects at the surfaces and buried interfaces in multilayer structures. In the context of semiconductors, extensive studies have been carried out using positron annihilation spectroscopy which are well documented [13]. Positron has been used as a charged probe for band bending structures near the interfaces between different materials due to the effect of electric field on the diffusion of positrons [14,15]. There are studies where positron has been used as interface sensitive probe in polar heterojunctions in addition to defects inside the bulk of the materials [16].

Beam based positron annihilation technique has been applied to study the surface and interfaces in multilayer structures like thin high k-dielectric films on Si substrates [17,18], metal-oxide semiconductor (MOS) structures [19], Si/SiO_2 interfaces [20] and many other multilayer structures. Most of the interest is centered on the characterization of grown-in defects [21–23]. There are several studies on internal field effects too, mainly at Si/SiO_2 interface [24–26].

We have prepared multilayer heterostructure of Cobalt-phthalocyanine (CoPc), Zinc-phthalocyanine (ZnPc) and Iron-phthalocyanine (FePc) having *p*-type, and copper-hexadecafluoro-phthalocyanine ($F_{16}CuPc$) having *n*-type characteristics. They include individual layers (*n* and *p*), bilayers (*p*–*n* and *p*–*p*) and multilayer like *n*–*p*–*n* on quartz substrates. Depth profile study has revealed characteristics features of the interfaces as well as type of defects in these multilayers. Positron mobility in organic molecular films (Phthalocyanines) has been determined and compared with effective charge carrier mobility measured from current density–voltage (*J*–*V*) characteristics. The positron data have been supplemented by Grazing incidence X-ray Diffraction (GIXRD) measurement on the multilayers. Positron diffusion modeling together with experimental data suggests the presence of disorder/defect at the interfaces which has a stronger influence on the positron systematics than the intrinsic electric field across organic–organic interfaces.

2. Experiment

Single layer and multilayer films of *n*-type ($F_{16}CuPc$) and *p*-type (CoPc, FePc and ZnPc) OSC materials have been prepared on quartz substrate by thermal evaporation using Hind high Vac thermal evaporation system (model no-12A4T) under vacuum better than 10^{-6} mbar. The substrate is cleaned by sonication with trichloroethylene, acetone and methanol separately for 5 min each before the deposition. The films are deposited at the substrate temperature of 100 °C and the deposition rate of 0.2 Å/s. The single layer films of *n*-type ($F_{16}CuPc$) and *p*-type (CoPc) material are 80 nm thick. The multilayer structures comprise bilayer of *p*–*n* (CoPc-$F_{16}CuPc$) and *p*–*p* (FePc-ZnPc) type and trilayer of *n*–*p*–*n* ($F_{16}CuPc$-CoPc-$F_{16}CuPc$) type OSC materials. The thickness of each film in bilayer and trilayer structures is 60 and 30 nm, respectively. The thickness of the films is measured by quartz crystal monitor.

The grown films have been characterized by GIXRD using PANalytical MRD system. The system studied are *n* and *p*-type films (80 nm) as well as *p*–*n* and *p*–*p* heterostructures (individual film thickness 60 nm). The measurements are carried out using CuK_α radiation of wavelength 0.15418 nm in out of plane geometry. The measurements are performed at varying grazing angles so as to probe the multilayer system as a function of depth. The high resolution theta-2-theta scan ranging from 0° to 30° in the step size of 0.0001° is carried out at each grazing angle.

The positron annihilation measurements have been carried out using the slow positron beam at Radiochemistry Division, Bhabha Atomic Research Centre. Positrons from a 50 mCi ^{22}Na source are moderated by a 1 μm tungsten foil and guided to the target chamber with the help of electric and magnetic field. The acceleration is done by floating the target to the required voltage. The depth dependent Doppler broadening measurements have been carried out in the energy range 200 eV–15 keV. A high efficiency high purity germanium detector with a resolution of 2.0 keV at 1332 keV photopeak of ^{60}Co is used for Doppler broadening measurements and approximately half a million counts are acquired under the 511 keV photopeak at each energy. The Doppler broadened annihilation γ-radiation is characterized by line shape parameters *S* and *W*. The *S*-parameter

mainly reflects the change due to positron annihilation with electrons having low momentum distribution, whereas, *W*-parameter reflects the annihilation from electrons with high momentum distribution. The ratio of integral counts within ∼2.0 keV energy window centered at 511 keV to the total photo peak area is used to evaluate the *S*-parameter, whereas, *W*-parameter is evaluated from 5.0 keV energy window in the wing region. The *S*–*W* correlation is examined to identify the nature and type of defects in these multilayers. VEPFIT analysis is used to fit the *S*-parameter profiles as a function of energy of the positrons. Positron mobility in organic layers is calculated from the fitted value of positron diffusion length.

The current density–voltage (*J*–*V*) measurements are carried out using in-plane electrode geometry. Two planar gold electrodes of length 3 mm, width 2 mm separated by 12 μm are thermally deposited onto the films using a metal mask and silver wires are attached to the gold pads with silver paint. The *J*–*V* measurements are carried out using Keithley 6487 picoammeter/voltage source and computer based data acquisition system.

3. Results

Figs. 1 and 2 show the GIXRD measurements for single layer (*n* and *p*) and bilayer (*p*–*n* and *p*–*p*) heterostuctures, respectively. The sharp peaks indicate that the films are crystalline. The *d*-spacing for *p*-type OSC material (CoPc) is 13.497 Å (2θ-angle 6.55°) and that of *n*-type OSC material ($F_{16}CuPc$) is 14.083 Å (2θ-angle 6.22°) as calculated from diffraction peaks for single layer films. In bilayer structures, different layers have been probed by varying the grazing angle. The dashed line (Fig. 2) corresponds to the organic–organic interface region i.e. it samples both the layers. In the case of *p*–*n* bilayer (Fig. 2a) two peaks obtained at different 2θ-angles correspond to *p* and *n*-type OSC materials. The 2θ-angles (*d*-spacings) for *p* and *n*-type materials are 6.62° and 6.22°, respectively consistent with the single layer films. For the *p*–*p* bilayer, sharp peaks are obtained at different grazing angles with slightly different 2θ-angle values (Fig. 2b) which correspond to *p*-type OSCs used in this bilayer. The 2θ-angles for the peaks are 6.87° and 6.80° and the *d*-spacing are 12.77 and 12.93 Å respectively. The *p*-type OSC materials used in *p*–*p* bilayer are different (FePc and ZnPc) from that used in *p*–*n* bilayer and single layer *p*-type film (CoPc). This has resulted in different values of 2θ-angles (*d*-spacing) in *p*–*p* bilayer.

Figs. 3 and 4 show the *S*-parameter variation as a function of positron energy for single layer films of *n* and *p*-type OSCs. A non-monotonic change in the *S*-parameter profile as a function of depth of the film is seen. The high value of *S*-parameter at a given depth is a signature of the presence of defects in that region. The single layer films of *n* and *p*-type OSC on quartz comprise of an interface between organic and inorganic (substrate) materials. The increase in *S*-parameter reflects the interfacial characteristics between the film and the substrate. The high value of *S*-parameter at the interface indicates the presence of open volume defects/domains (trap centers) and reveals the microstructure variation between organic and inorganic materials (substrate) as indicated by the subsequent fall in *S*-parameter. The epitaxial relation between the film and the substrate is important in crystallographic sense as well as for growth behavior. The organic molecules have large anisotropy and internal degrees of freedom due to low symmetry and extended size. The effect of size difference of unit cells of organic molecules and the inorganic substrate as well as molecule–substrate interaction lead to translational and orientational domains, which are the sources of disorders [27]. In addition, growth of the films is accomplished by the interplay of molecule–molecule and molecule–substrate interaction [28].

Figs. 5 and 6 show *S*-parameter profiles for *p*–*n* and *p*–*p* bilayers. These bilayers comprise of organic–organic and organic–inorganic (substrate) interfaces. Enhancement in the *S*-parameter is seen at the organic–inorganic interfaces in both the cases (*p*–*n* and *p*–*p*) similar to the observation in single layer films. However, there is a marked difference

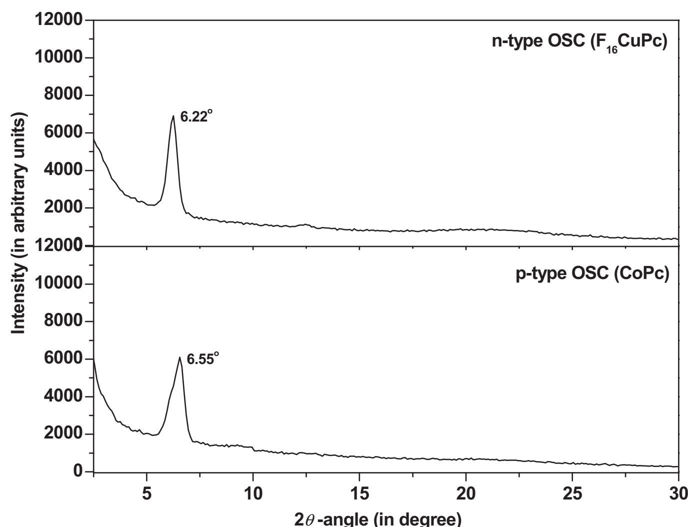

Fig. 1. GIXRD data for single layer films of *n* and *p*-type OSC materials on quartz substrate.

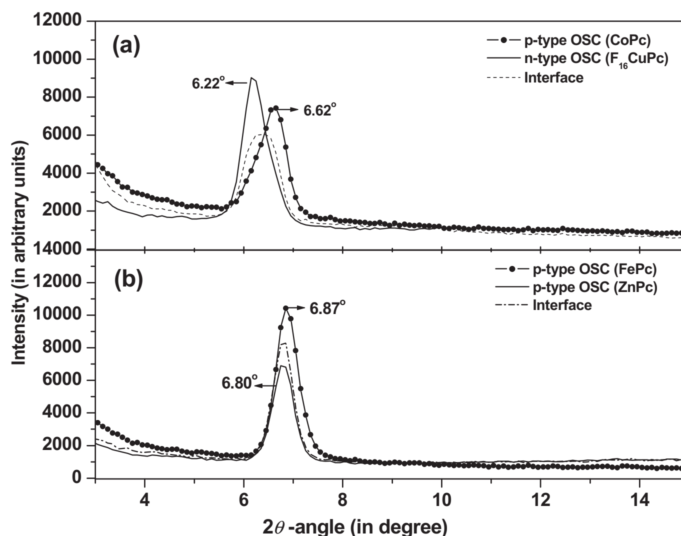

Fig. 2. GIXRD data for bilayer layer films of *p*–*n* and *p*–*p*-type OSC materials on quartz substrate.

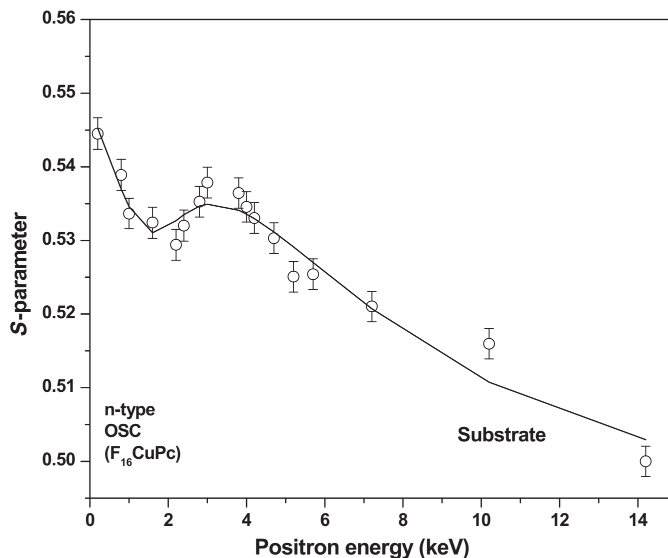

Fig. 3. Variation of *S*-parameter as a function of positron energy (keV) in single layer film of *n*-type OSC material deposited on quartz substrate. The solid line represents the best fit to data using VEPFIT.

in *S*-parameter profiles in the region corresponding to organic layers. The region corresponding to organic-organic interface in the two types of heterostructures show different features. The *S*-parameter shows sharp increase at a depth corresponding to the interface between *p* and *n*-type OSCs (in *p*–*n* bilayer) which is absent in the case of *p*–*p* interface (in *p*–*p* bilayer) that shows a smoothly varying *S*-parameter profile. As mentioned earlier, *p*–*n* interface has an intrinsic electric field directed in the beam direction which is absent in the *p*–*p* interface. It is tempting to suggest that the intrinsic electric field is responsible for the increased *S*-parameter at the interface in *p*–*n* bilayer. It is to be noted that the difference in *d*-spacing for the constituents in *p*–*n* bilayer is larger compared to that of *p*–*p* bilayer. This incoherency/lattice mismatch at the interface is expected to produce defects due to local molecular ordering at the junction as well as strain at the interface in *p*–*n* bilayer as compared to *p*–*p* bilayer.

The *S*-parameter profile as a function of depth for *n*–*p*–*n* heterostructure is shown in Fig. 7. The *n*–*p*–*n* trilayer comprises of two organic–organic (*n*–*p* and *p*–*n*) and organic–inorganic (*n*-type OSC and substrate) interfaces. The *S*-parameter profile shows similar features as observed in the case of *p*–*n* bilayer i.e. enhancement of *S*-parameter at all the interfaces. The enhancement in *S*-parameter at the organic–organic interfaces in *p*–*n* and *n*–*p*–*n* heterostructures is expected to be a cumulative effect of the presence of defects and intrinsic electric field. However,

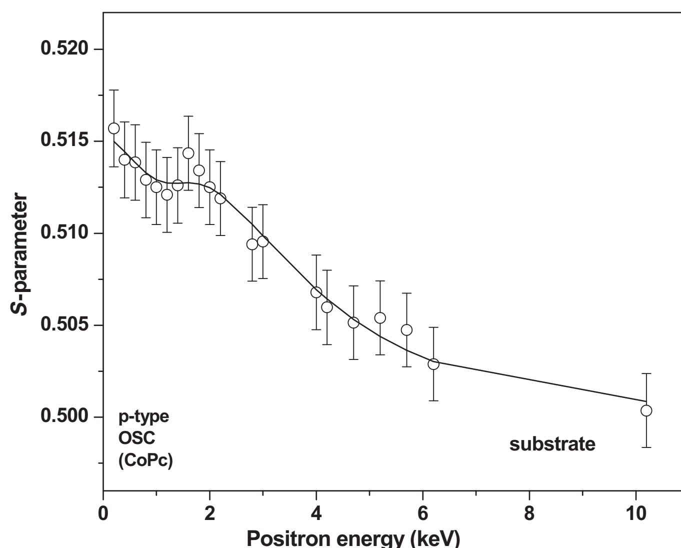

Fig. 4. Variation of *S*-parameter as a function of positron energy (keV) in single layer film of *p*-type OSC material deposited on quartz substrate. The solid line represents the best fit to data using VEPFIT.

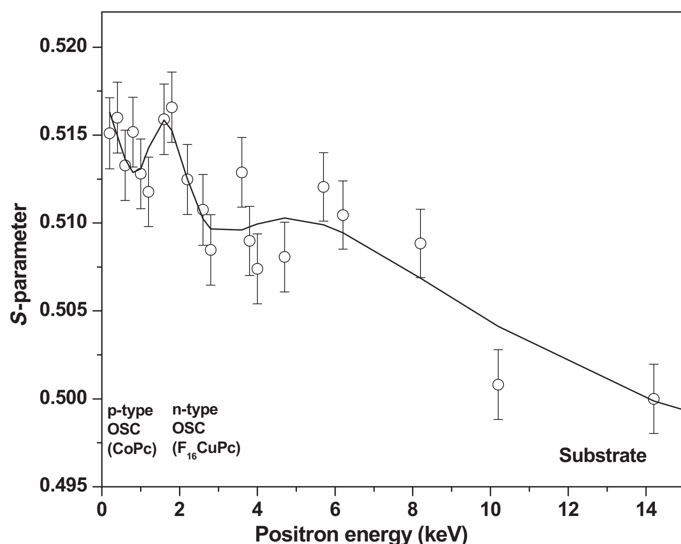

Fig. 5. Variation of *S*-parameter as a function of positron energy (keV) in *p*–*n* bilayer deposited on quartz substrate. The solid line represents the best fit to data using VEPFIT.

positron diffusion modeling in the presence and absence of electric field is suggestive of the fact that electric field across the interface need not necessarily help localize positrons at the interfaces, a discussion on which is given in latter section.

4. Discussion

4.1. Positron diffusion analysis

Depth dependent *S*-parameter profiles have been fitted using VEPFIT analysis to evaluate the characteristics of heterostructures with depth. VEPFIT analysis involves solving positron diffusion equation taking into account the positron diffusion, trapping and annihilation in the medium [29]. The positron diffusion equation is given as,

$$D + \frac{d^2 c(z)}{dz^2} - \frac{d}{dz}(v_d c(z)) + I(z) - \kappa_t n_t c(z) - \lambda_b c(z) = 0 \quad (1)$$

where, $c(z)$ is the time averaged positron density at a certain depth z below the solid surface, v_d is the drift velocity of positrons, $I(z)$ is the positron stopping rate at depth z, n_t is defect density, κ_t is rate constant for positron trapping at defects, λ_b is the bulk annihilation rate and D_+ is positron diffusion coefficient. The drift velocity is the function of

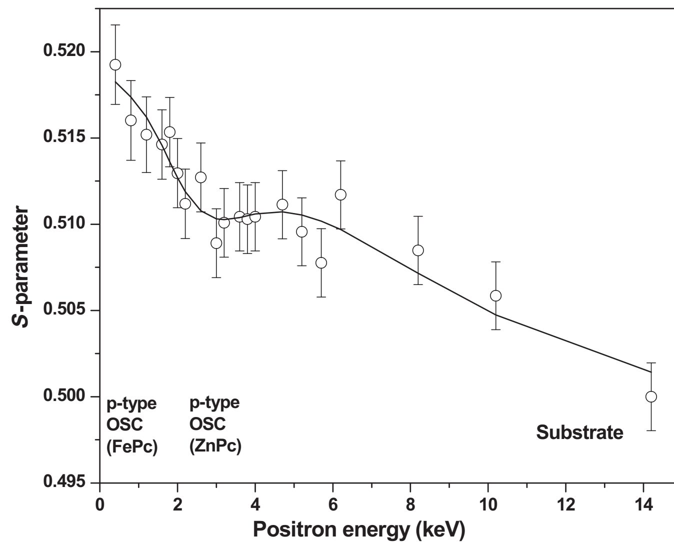

Fig. 6. Variation of *S*-parameter as a function of positron energy (keV) in *p–p* bilayer deposited on quartz substrate. The solid line represents the best fit to data using VEPFIT.

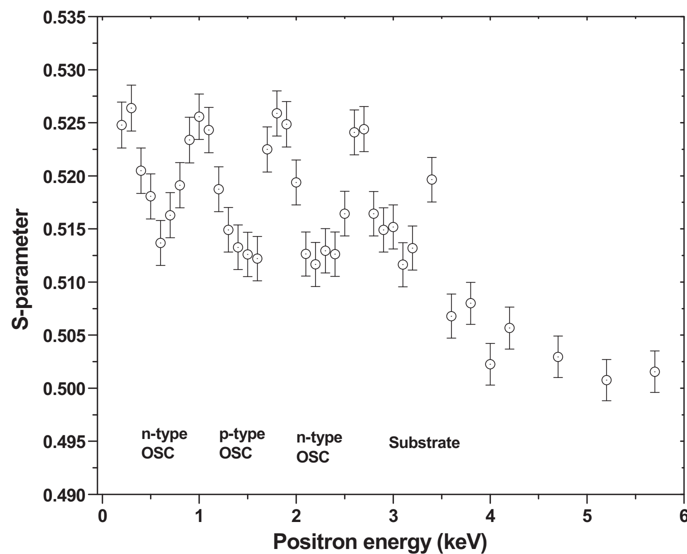

Fig. 7. Variation of *S*-parameter as a function of positron energy (keV) in *n–p–n* trilayer.

electric field and is expressed as: $v_d = \mu E$; where, μ is the mobility of positron and E is the electric field strength.

The depth dependent implantation rate of thermalised positrons is obtained by Makhovian distribution $P(z)$, given by,

$$P(z) = \frac{m}{z_0^m} z^{m-1} exp\left[-\left(\frac{z}{z_0}\right)^m\right] \tag{2}$$

where, m is the shape parameter of $P(z)$, z_0 is given by, $z_0 = AE^n/\rho$, where, z_0 is expressed in nm, E is the positron energy in keV, ρ is the density of medium in g/cm^3 and A is a material dependent constant. In the present work, values of A, m, n and ρ are taken as 40 nm g/(keV)^n cm^3, 1.9, 1.6 and 1.7 g/cm^3 for OSCs and 2.33 g/cm^3 for quartz substrate, respectively. The observed S-parameter profiles are then fitted by the relation:

$$S(E) = S_s F_s + \sum_{i=1}^{n} S_i F_i \tag{3}$$

where, S_S, S_i, F_S and F_i are the characteristics value of S-parameters and fraction of positrons annihilating at the surface and in different layers, respectively. The fast non-iterative calculation scheme is used to solve the diffusion equation to calculate the time averaged positron density in the medium. The average positron density is then used to extract diffusion length and the fraction of positrons annihilating at various depths taking into account the various boundary conditions for the diffusing positrons. The

Table 1
Fitted values of *S*-parameter and positron diffusion length (L_+) in single layer of *n* and *p*-type OSCs.

Sample	Layer 1		Layer 2		Layer 3	
	S1	$L_+(1)$ (nm)	S2	$L_+(2)$ (nm)	S3	$L_+(3)$ (nm)
n-type	0.51198	30	0.54468	0.2	0.5000	320
p-type	0.50742	35	0.51533	0.2	0.5000	110

Table 2
Fitted values of *S*-parameter and positron diffusion length (L_+) in *p*–*n* and *p*–*p* bilayers.

Sample	Layer 1		Layer 2		Layer 3		Layer 4		Layer 5	
	S1	$L_+(1)$ (nm)	S2	$L_+(2)$ (nm)	S3	$L_+(3)$ (nm)	S4	$L_+(4)$ (nm)	S5	$L_+(5)$ (nm)
pn type	0.48532	37	0.54303	0.1	0.44971	62	0.51752	0.2	0.4970	500
pp type	0.51625	31	–	–	0.506181	27	0.51619	0.2	0.4970	350

above information can be used to calculate *S*-parameter and positron diffusion length at various depths of the sample.

The fitted *S*-parameter profiles for single layer as well as bilayers (*p*–*n* and *p*–*p* type) are represented by solid lines in Figs. 3–6. The fitted parameters are shown in Tables 1 and 2. The best fit could be obtained by taking an interface layer between OSC and the substrate in all cases. In *p*–*n* bilayer, unlike the *p*–*p* case, an additional interface layer between the *p* and *n*-type OSC has to be considered for fitting the data. The obtained diffusion lengths are seen to be in the range of 30–40 nm in organic layers and 0.1–0.2 nm in the interfaces. The *S*-parameters in the interface layers are seen to be higher, and, together with the observed short diffusion length clearly indicate strong positron localization at the interfaces.

In the case of *p*–*n* bilayer the presence of an intrinsic electric field at the interface of *p* and *n* type OSC layers is expected. However, in the fitting described above we have not considered the presence of electric field due to lack of knowledge on the exact value of the field which is evaluated from current–voltage characteristics and in situ spectroscopic measurements. In order to examine the influence of electric field alone or together with the presence of defects at the interface on the positron systematics, we have simulated the *S*-parameter profile. The model system consists of a top *p*-type layer, followed by an interface layer and *n*-type layer of infinite thickness. The presence of defects is represented by high *S*-parameter and short diffusion length of positrons at the interface. Similarly, the absence of defects is represented by taking the interface layer *S*-parameter and diffusion length identical to that of the top layer.

Fig. 8 shows the simulated profiles of *S*-parameter. Fig. 8a shows the effect of electric field at the interface in the presence of defects. Presence of electric field in the direction of the beam (in the present case) drifts the positrons away from the interface. Effectively, positrons see the bottom layer at lower implantation energy or depth leading to the observed profile. It can be seen that the electric field has marginally but distinctly modified the profile keeping the effect of defects (positron trapping at the interface) dominant. Fig. 8b shows the effect of electric field at the interface in the absence of defects. The profile indicates that the electric field alone cannot generate the observed experimental profile in the absence of defects at the interface. It is clear from this modeling that the presence of defects due to epitaxial relation between the materials is the dominant feature leading to enhanced trapping of positrons at the interface.

In the case of *n*–*p*–*n* trilayer, fitting could not be done due to the presence of large number of layers (seven layers) including the interfaces between organic materials. However, sharp features in experimental *S*-parameter profile are indicative of interfaces between *p* and *n*-type materials similar to that observed in *p*–*n* bilayer. It may be mentioned that the electric fields at the two organic interfaces (*n*–*p* and *p*–*n*) are in opposite direction. We believe, this has effectively improved the depth resolution especially for the middle layer (*p*-type) owing to the modification of implantation profile.

4.2. S–W analysis

Depth dependent Doppler broadening measurement provides the characteristic features of the layers as a function of depth. The *S*-parameter profiles for single and multilayers (*n*, *p*, *p*–*n*, *p*–*p* and *n*–*p*–*n*) have indicated the presence of interfaces with significant defects at the junction of different organic as well as organic and inorganic materials. However, the type and nature of defects at the interfaces can be discerned from *S*–*W* analysis which involves simultaneous analysis of *S* and *W* parameters. This helps in recognizing positron annihilation states in the system. Fig. 9 shows the *S*–*W* curve for *p*–*p* and *p*–*n* bilayers. The *S* and *W* values have been normalized with respect to quartz substrate. Each *S* and *W* value corresponds to a particular depth of the sample. The quartz substrate is represented by $S = W = 1$. The *S*–*W* curves for *p*–*p* and *p*–*n* bilayers show different slopes which indicate the presence of different type of defects in these heterostructures. In the case of *p*–*n* bilayer, *S*–*W* points corresponding to different depths lie on the line L2 (shown in Fig. 9) indicating the presence of similar type of defects throughout the bilayer. However, defects at organic–organic interface are more as

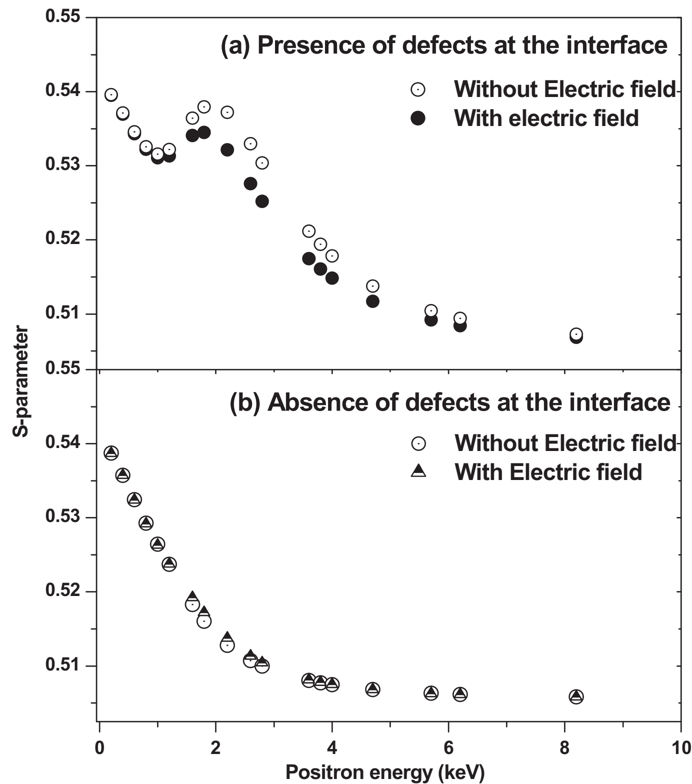

Fig. 8. *S*-parameter profiles for a *p–n* heterostructure as obtained from Positron diffusion modeling considering different scenarios for the effect of defects and electric field at the interface; (a) effect of electric field at the interface in the presence of defects; (b) effect of electric field at the interface in the absence of defects.

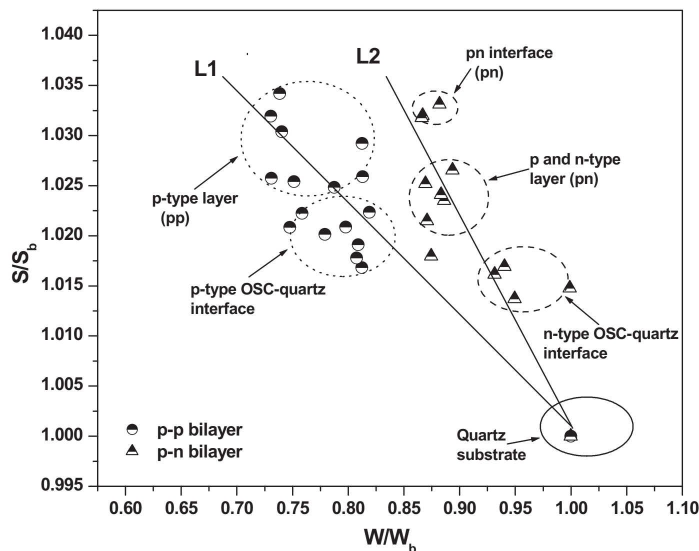

Fig. 9. *S–W* correlation for *p–n* and *p–p* bilayers.

compared to bulk layer. Similarly, in the case of *p–p* bilayer, only one kind of defects exist throughout the depth, however, the *S–W* curve (line L1) shows the absence of interface between *p*-type materials. Fig. 10 shows the *S–W* curves for *p–p*, *p–n* and *n–p–n* together. It is seen that the slope of *S–W* curves of *p–n* and *n–p–n* multilayer is same, but different from *p–p* bilayer. It indicates that the nature of defects in *p–n* and *n–p–n* is similar and distinct from *p–p* bilayer. The difference in the nature of defects in these multilayers is due to the presence of different

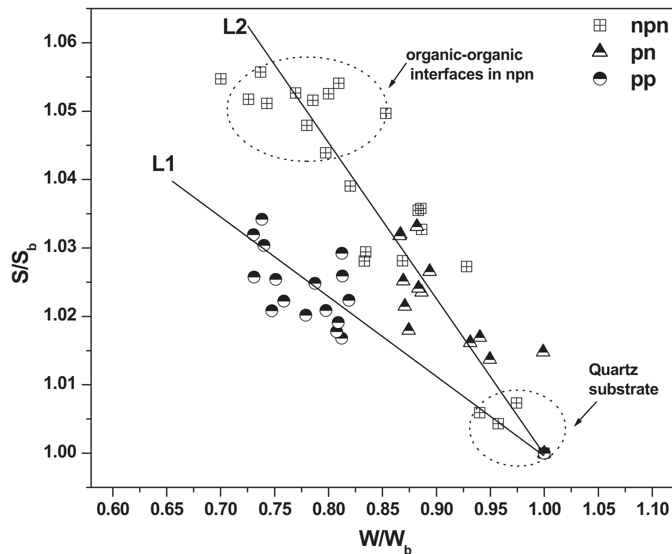

Fig. 10. *S–W* correlation for *p–n*, *p–p* and *n–p–n* multilayers.

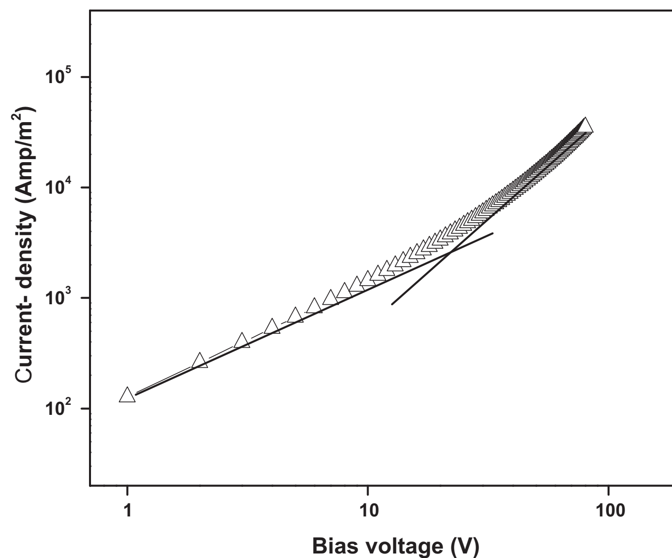

Fig. 11. Current density–voltage (*J–V*) characteristics in single layer OSC film.

organic materials (*n* and *p*-type). The *S–W* curves for *n–p–n* trilayer shows the presence of more defects at the organic interfaces as compared to *p–n* bilayers. This can be attributed to different morphology of the layers owing to the different thickness of the layers in *p–n* and *n–p–n* multilayers. Thus, *S–W* mapping has revealed the effect of organic materials as well as thickness of layers on the defect microstructure in multilayers.

4.3. Mobility of positrons and charge carriers in OSC layers

The mobility of positrons in a medium depends on its microstructure due to the tendency of positrons to get trapped at the structural defects. The positron diffusion length obtained from VEPFIT analysis can be used to calculate positron mobility in OSC layers. The positron diffusion length L_+ and diffusion coefficient D_+ are related as,

$$L_+ = \sqrt{D_+ \tau} \tag{4}$$

where, τ is positron lifetime in the material. The diffusion coefficient can be used to calculate positron diffusion mobility in the material using Nernst–Einstein relation,

$$D_+ = \mu_+ k_B T / e \tag{5}$$

where, μ_+ is positron diffusion mobility, k_B is Boltzman's constant, T is temperature and e is electronic charge. Coincident Doppler broadening studies have shown that positron/Ps do not interact with the metal ion in

phthalocyanines. The positron lifetime in bulk of phthalocyanine is reported in the range 0.290–0.330 ns [30]. The positron diffusion coefficient is calculated using Eq. (4), taking into account the positron diffusion length of 35 nm as calculated from VEPFIT analysis and positron lifetime as 300 ps. The diffusion mobility (μ_+) of positron estimated using Einstein's relation (Eq. (5)) is 1.6 cm^2/Vs.

We have measured the effective mobility of charge carriers from *J–V* characteristics in organic layers. The measured *J–V* characteristics in *n*-type OSC single layer film is shown in Fig. 11. At low voltage, *J–V* characteristics represent ohmic conduction. At higher voltages the transport mechanism is governed by space charge limited conduction (SCLC). In the SCLC region, charge transport is governed via deep traps existing in the organic layers. These deep traps can be generated due to the presence of structural defects in the organic layers [31]. In the presence of deep traps (defects), *J–V* characteristics in SCLC region is given by:

$$J = \frac{9\varepsilon_0\varepsilon_r\mu\theta}{8d^3}V^2 \tag{6}$$

where, ε_0 is the permittivity of free space, μ is the charge carrier mobility, ε_r is the static dielectric constant of the material and θ is described as ratio of density of free carriers to the density of total charge carriers, i.e. $\theta = p/(p + p_t)$ where, p is the free carrier density and p_t is the density of trapped carriers. In the presence of defects the value of θ is less than 1 and approaches a maximum value of 1 in the absence of any defect. Using the slope of *J–V* plots for *n*-type OSC single layer film and the literature value of $\varepsilon_0\varepsilon_r$ as 2.43×10^{-11} F/m, the effective mobility of charge carriers, $\mu\theta$ in organic layer is calculated as 3.5 cm^2/Vs. The effective mobility ($\mu\theta$) of charge carriers decreases with the increase in defect density of the medium. The mobility of positrons which is also strongly dependent on the structural defects in the materials is seen to be comparable to the effective mobility ($\mu\theta$) of charge carriers determined from the *J–V* characteristics. It is an interesting observation and it offers the possibility to determine defect (trap) density and charge conductivity in organic thin films by measuring the positron mobility. It may, however, be mentioned that the dynamic behavior of positron and charge carrier are different in a medium due to the difference in the scattering mechanism and nature of delocalization of their wave functions. More studies on variety of OSC materials are necessary to ascertain stronger correlation between positron mobility and effective mobility of charge carriers.

5. Conclusion

We have carried out defect depth profiling in OSC multilayers of varying thickness to characterize buried interfaces and microstructure of the layers. The variation of *S*-parameter as a function of depth shows a non-monotonic change represented by an increase at a depth corresponding to the junction between organic–organic and organic–inorganic materials. VEPFIT analysis reveals the presence of interface with high *S*-parameter and short diffusion length between the organic–organic and organic–inorganic materials. The high value of *S*-parameter shows the presence of structural defects owing to the incoherency or lattice mismatch between the layers. The organic–organic interface is seen to be absent in *p–p* bilayer where lattice mismatch is found to be less compared to *p* and *n*-type materials in *p–n* and *n–p–n* multilayers. We have also examined the nature and type of defects in these multilayers by simultaneous mapping of *S* and *W* parameters. The *S–W* correlation shows the presence of different type of defects in *p–p* bilayer as compared to *p–n* and *n–p–*n reflected from the different slopes of the *S–W* curves. The effect of type of organic materials and layer thickness on defect microstructure is also observed.

Positron systematics at charged organic interfaces has been examined using positron diffusion modeling to understand the influence of intrinsic electric field and structural defects present at the interfaces. It has been shown that the defect/disorder at the interface has more influence on the positron systematics than the built in electric field. While the interface defects tend to localize the positrons, the electric field facilitates drift of positron away from the interface in the direction of the electric field. The positron diffusion length calculated from VEPFIT fitting is used to calculate positron mobility in organic layers which is influenced by structural defects. Positron mobility obtained in organic layers is seen to be comparable to effective mobility of charge carrier measured from *J–V* characteristics. This is an interesting observation and can be used to evaluate trap density as well as charge conductivity in organic layers. Our study reveals that the defect profiling using positron annihilation technique can be used as a non destructive tool to characterize organic devices at the early stage of fabrication and can give preliminary knowledge of trap density and charge conductivity in organic layers.

References

[1] A. Dodabalapur, H.E. Katz, L. Torsi, R.C. Haddon, Science 269 (1995) 1560.
[2] C.W. Tang, S.A. Vanslyke, Appl. Phys. Lett. 51 (1987) 913.
[3] P. Peumans, S.R. Forrest, Appl. Phys. Lett. 79 (2001) 126.
[4] C.W. Tang, S.A. Vanslyke, Appl. Phys. Lett. 48 (1986) 153.
[5] L. Ma, J. Pyo, S. Liu, Y. Yamg, Appl. Phys. Lett. 80 (2002) 362.
[6] P. Ruden, Nat. Mater. 10 (2011) 8.
[7] M. Grobosch, M. Knupfer, Appl. Phys. J. 4 (2011) 8.
[8] A.A. Virkar, S. Mannsfeld, Z. Bao, N. Stingelin, Adv. Mater. 22 (2010) 3857.
[9] A. Tada, Y. Geng, Q. Wei, K. Hashimoto, K. Tajima, Nat. Mater. 10 (2011) 450.
[10] R.R. Lunt, K. Sun, M. Kröger, J.B. Benziger, S.R. Forrest, Phys. Rev. B 83 (2011) 064114.
[11] G. Koller, S. Berkebile, J.R. Krenn, F.P. Netzer, M. Oehzelt, T. Haber, R. Resel, M.G. Ramsey, Nano Lett. 6 (2006) 1207.
[12] T. Schmitz-Hubsch, F. Sellam, R. Staub, M. Torker, T. Fritz, Ch. Kubel, K. Leo, Surf. Sci. 445 (2000) 358.
[13] R. Krause-Rehberg, H.S. Leipner, Positron Annihilation in Semiconductors: Defect Studies, Springer-Verlag, Berlin, Heidelberg, New York, 1999.
[14] A. van Veen, H. Schut, M. Clement, J.M.M. De Nijs, A. Kruseman, M.R. Ijpma, Appl. Surf. Sci. 85 (1995) 216.
[15] A. Uedono, T. Naito, T. Otsuka, K. Shiraishi, K. Yamabe, S. Miyazaki, H. Watanabe, N. Umezawa, T. Chikyow, Y. Akasaka, S. Kamiyama, Y. Nara, K. Yamada, J. Appl. Phys. 100 (2006) 064501.
[16] I. Makkonen, A. Snicker, M.J. Puska, J.M. Mäki, F. Tuomisto, Phys. Rev. B 82 (2010) 041307.

[17] A. Uedono, T. Naito, T. Otsuka, K. Ito, K. Shiraishi, K. Yamabe, S. Miyazaki, H. Watanabe, N. Umezawa, T. Chikyow, T. Ohdaira, R. Suzuki, Y. Akasaka, S. Kamiyama, Y. Nara, K. Yamada, Jpn. J. Appl. Phys. 46 (2007) 3214.
[18] A. Uedono, K. Ikeuchi, K. Yamabe, T. Ohdaira, M. Muramatsu, R. Suzuki, A.S. Hamid, T. Chikyow, K. Torii, K. Yamada, J. Appl. Phys. 98 (2005) 023506.
[19] A. Uedono, S. Tanigawa, Y. Ohji, Phys. Lett. A 133 (1988) 82.
[20] H. Kauppinen, C. Corbel, L. Liszkay, T. Laine, J. Oila, K. Saarinen, P. Hautojärvi, M-F. Barthe, G. Blondiaux, J. Phys.: Condens. Matter 9 (1997) 10595.
[21] D.T. Britton, P. Willutzki, T.E. Jackman, P. Mascher, J. Phys.: Condens. Matter 4 (1992) 8511.
[22] T.E. Jackman, G.C. Aers, M.W. Denhoff, P.J. Schulz, Appl. Phys. A 49 (1989) 335.
[23] P.G. Coleman, N.B. Chilton, J.A. Baker, J. Phys.: Condens. Matter 2 (1990) 9355.
[24] D.T. Britton, P. Willutzki, W. Triftshäuser, E. Hammerl, W. Hansch, I. Eisele, Appl. Phys. A 58 (1994) 389.
[25] P. Asoka-Kumar, K.G. Lynn, D.O. Welch, J. Appl. Phys. 76 (1994) 4935.
[26] D.L. Smith, C. Smith, P.C. Rice-Evans, H.E. Evans, S. Romani, J.H. Evans, J. Phys.: Condens. Matter 3 (1991) 3205.
[27] W. Brutting, Physics of Organic semiconductors, WILEY-VCH Verlag GmbH & Co. KGaA, Weinheim, 2008.
[28] A.K. Debnath, S. Samanta, A. Singh, D.K. Aswal, S.K. Gupta, J.V. Yakhmi, S.K. Deshpande, A.K. Poswal, C. Surgers, Physica E 41 (2008) 154.
[29] A. van Veen, H. Schut, J. De. Vries, R.A. Hakvoort, M.R. Ijpma, AIP Conf. Proc. 218 (1990) 171.
[30] Y. Ito, T. Suzuki, Rad. Phys. Chem. 58 (2000) 743.
[31] S. Samanta, A. Singh, A.K. Debnath, D.K. Aswal, S.K. Gupta, J.V. Yakhmi, S. Singh, S. Basu, S.K. Deshpande, J. Appl. Phys. 104 (2008) 073717.